MOX–Report No. 24/2012

hpVersion Composite Discontinuous Galerkin Methods for Elliptic Problems on Complicated Domains

Antonietti, P.F.; Giani, S.; Houston, P.

MOX, Dipartimento di Matematica "F. Brioschi"
Politecnico di Milano, Via Bonardi 9 - 20133 Milano (Italy)

mox@mate.polimi.it http://mox.polimi.it

hp–Version Composite Discontinuous Galerkin Methods for Elliptic Problems on Complicated Domains

Paola F. Antonietti[♮], Stefano Giani[♭], Paul Houston[†]

May 15, 2012

[♮] MOX–*Modeling and Scientific Computing*, Dipartimento di Matematica, Politecnico di Milano, Piazza Leonardo da Vinci 32, 20133 Milano, Italy, paola.antonietti@polimi.it.

[♭] School of Mathematical Sciences, University of Nottingham, University Park, Nottingham NG7 2RD, UK, Stefano.Giani@nottingham.ac.uk.

† School of Mathematical Sciences, University of Nottingham, University Park, Nottingham NG7 2RD, UK, Paul.Houston@nottingham.ac.uk.

Keywords: Composite finite element methods, discontinuous Galerkin methods, *hp*–version finite element methods

Abstract

In this paper we introduce the *hp*–version discontinuous Galerkin composite finite element method for the discretization of second–order elliptic partial differential equations. This class of methods allows for the approximation of problems posed on computational domains which may contain a huge number of local geometrical features, or micro-structures. While standard numerical methods can be devised for such problems, the computational effort may be extremely high, as the minimal number of elements needed to represent the underlying domain can be very large. In contrast, the minimal dimension of the underlying composite finite element space is *independent* of the number of geometric features. The key idea in the construction of this latter class of methods is that the computational domain Ω is no longer resolved by the mesh; instead, the finite element basis (or shape) functions are adapted to the geometric details present in Ω. In this article, we extend these ideas to the discontinuous Galerkin setting, based on employing the *hp*–version of the finite element method. Numerical experiments highlighting the practical application of the proposed numerical scheme will be presented.

1 Introduction

The numerical approximation of partial differential equations (PDEs) posed on complicated domains which contain 'small' geometrical features, or so-called micro-structures, is of vital importance in engineering applications. In such situations, an extremely large number of elements may be required for a given mesh generator to produce even a 'coarse' mesh which

adequately describes the underlying geometry. With this in mind, the solution of the resulting system of equations emanating, for example, from a finite element discretization of the underlying PDE of engineering interest on the resulting 'coarse' mesh, may be impractical due to the large numbers of degrees of freedom involved. Moreover, since this initial 'coarse' mesh already contains such a large number of elements, the use of efficient multi-level solvers, such as multigrid, or domain decomposition, using, for example, Schwarz-type preconditioners, may be difficult, as an adequate sequence of 'coarser' grids which represent the geometry are unavailable.

In recent years, a new class of finite elements, referred to as Composite Finite Elements (CFEs), have been developed for the numerical solution of partial differential equations, which are particularly suited to problems characterized by small details in the computational domain or micro-structures; see, for example, [11, 10], for details. This class of methods are closely related to the Shortley-Weller discretizations developed in the context of finite difference approximations, cf. [17]. The key idea of CFEs is to exploit general shaped element domains upon which elemental basis functions may only be locally piecewise smooth. In particular, an element domain within a CFE may consist of a collection of neighbouring elements present within a standard finite element method, with the basis function of the CFE being constructed as a linear combination of those defined on the standard finite element subdomains; see below for further details. In this way, CFEs offer an ideal mathematical and practical framework within which finite element solutions on (coarse) aggregated meshes may be defined. To date, CFEs have been developed in the context of h–version conforming finite element methods. In this article, we consider the generalisation of this class of schemes to the case when hp–version discontinuous Galerkin composite finite element methods (DGCFEMs) are employed. For simplicity of presentation, here we consider DGCFEMs as a numerical solver for a simple second–order elliptic PDE posed on a computational domain which contains small details, or micro-structures. The application of this approach within multi-level solvers will be considered elsewhere. We point out that the general philosophy of CFE methods is to construct the underlying finite element spaces based on first generating a hierarchy of meshes, such that the finest mesh does indeed provide an accurate representation of the underlying computational domain, followed by the introduction of appropriate prolongation operators which determine how the finite element basis functions on the coarse mesh are defined in terms of those on the fine grid. A closely related method based on employing a fictitious boundary approach is developed by Larson & Johansson in [13]; cf., also the work presented in the series of articles [6, 7, 8].

The structure of this article is as follows. In Section 2, we introduce the model problem and state the necessary assumptions on the computational domain Ω. Section 3 introduces the composite finite element spaces considered in this article, based on exploiting the ideas developed in the series of articles [11, 10, 14]. In Section 4 we formulate the DGCFEM; the stability and *a priori* analysis of the proposed method is then undertaken in Sections 5, 6, and 7. In Section 8 we briefly outline how the proposed DGCFEM may be efficiently implemented. The practical performance of the DGCFEM for a range of two– and three–dimensional problems is studied in Section 9. Finally, in Section 10 we summarize the work presented in this paper and draw some conclusions.

2 Model problem

In this article we consider the following model problem: given $f \in L_2(\Omega)$, find u such that

$$-\Delta u = f \quad \text{in } \Omega, \tag{1}$$
$$u = 0 \quad \text{on } \partial\Omega. \tag{2}$$

Here, Ω is a bounded, connected Lipschitz domain in $\mathbb{R}^d$, $d > 1$, with boundary $\partial\Omega$; in particular, it is assumed that Ω is a 'complicated' domain, in the sense that it contains small details or micro-structures. With this in mind, throughout this article, we assume that Ω is such that the following extension result holds.

Theorem 2.1. *Let Ω be a domain with a Lipschitz boundary. Then there exists a linear extension operator $\mathfrak{E} : H^s(\Omega) \to H^s(\mathbb{R}^d)$, $s \in \mathbb{N}_0$, such that $\mathfrak{E}v|_\Omega = v$ and*

$$\|\mathfrak{E}v\|_{H^s(\mathbb{R}^d)} \leq C\|v\|_{H^s(\Omega)},$$

where C is a positive constant depending only on s and Ω.

Proof. See Stein [18, Theorem 5, p. 181] □

Remark 2.2. *We note the conditions on the domain Ω may be weakened. Indeed, [18] only requires that Ω is a domain with a minimally smooth boundary; moreover, the extension of Theorem 2.1 to domains which are simply connected, but may contain micro-scales, is considered in [16].*

3 Construction of the composite finite element spaces

In order to construct the CFE space, we proceed in the following steps; we point out that the discussion presented in this section is based on the articles by Sauter and co-workers; see, for example, [11, 10, 14]. In Section 3.1, we construct a hierarchy of finite element meshes which can be used to describe a complicated domain $\Omega \subset \mathbb{R}^d$; for simplicity of presentation, we assume that $d = 2$, though the general approach naturally generalizes to higher–dimensional domains. Having constructed a suitable sequence of meshes, in Section 3.2 we introduce the corresponding CFE space, which consists of piecewise discontinuous polynomials, defined on 'generalized' elemental domains.

3.1 Finite element meshes

In this section we outline a general strategy to generate a hierarchy of finite element meshes, cf. [11]. We point out that any such hierarchy of meshes may be employed within this framework.

To begin, we first need to construct a sequence of *reference* meshes, which we shall denote by $\hat{\mathcal{T}}_{h_i}$, $i = 1, \ldots, \ell$. We assume that the reference meshes are nested, in the sense that every element $\hat{\kappa}_i \in \hat{\mathcal{T}}_{h_i}$, $i = 1, \ldots, \ell - 1$, is a parent of a subset of elements which belong to the finer mesh $\hat{\mathcal{T}}_{h_j}$, where $j = i + 1, \ldots, \ell$. To this end, we proceed as follows: we define a coarse conforming shape–regular mesh $\hat{\mathcal{T}}_H = \{\hat{\kappa}\}$, consisting of (standard) closed disjoint elements $\hat{\kappa}$. By *standard* element domains, we mean quadrilaterals/triangles in two dimensions ($d = 2$), and tetrahedra/hexahedra when $d = 3$. Here, we assume that $\hat{\mathcal{T}}_H$ is an *overlapping* mesh

is the sense that it does *not* resolve the boundary of the computational domain Ω. More precisely, we assume that $\hat{\mathcal{T}}_H$ satisfies the following condition:

$$\Omega \subset \Omega_H = \left(\bigcup_{\hat{\kappa} \in \hat{\mathcal{T}}_H} \hat{\kappa} \right)^\circ \quad \text{and} \quad \hat{\kappa}^\circ \cap \Omega \neq \emptyset \ \forall \hat{\kappa} \in \hat{\mathcal{T}}_H,$$

where, for a closed set $D \subset \mathbb{R}^d$, D° denotes the interior of D, cf. [14], for example. The finite element mesh $\hat{\mathcal{T}}_H$ should be viewed as having a granularity that is affordable for which to solve our underlying problem, though is far too coarse to actually represent the underlying geometry Ω.

Given $\hat{\mathcal{T}}_H$, we may now construct a sequence of successively refined (nested) computational meshes using the following algorithm.

Algorithm 3.1 (Refine Mesh)**.**

1. *Set $\hat{\mathcal{T}}_{h_1} = \hat{\mathcal{T}}_H$, and the mesh counter $\ell = 1$.*
2. *Set $\hat{\mathcal{T}}_{h_{\ell+1}} = \emptyset$.*
3. *For all $\hat{\kappa} \in \hat{\mathcal{T}}_{h_\ell}$ do*
   (a) *If $\hat{\kappa} \subset \Omega$ then $\hat{\mathcal{T}}_{h_{\ell+1}} = \hat{\mathcal{T}}_{h_{\ell+1}} \bigcup \{\hat{\kappa}\}$;*
   (b) *Otherwise refine $\hat{\kappa} = \bigcup_{i=1}^{n_{\hat{\kappa}}} \hat{\kappa}_i$; here, $n_{\hat{\kappa}}$ will depend on both the type of element to be refined, and the type of refinement (isotropic/anisotropic) undertaken; for the standard red refinement of a triangular element $\hat{\kappa}$, we have that $n_{\hat{\kappa}} = 4$. For $i = 1, \ldots, n_{\hat{\kappa}}$, if $\hat{\kappa}_i \cap \Omega \neq \emptyset$ then set $\hat{\mathcal{T}}_{h_{\ell+1}} = \hat{\mathcal{T}}_{h_{\ell+1}} \bigcup \{\hat{\kappa}_i\}$.*
4. *Perform additional refinement of elements in $\hat{\mathcal{T}}_{h_{\ell+1}}$ to undertake appropriate mesh smoothing; cf. Remark 3.2 below.*
5. *If the reference mesh $\hat{\mathcal{T}}_{h_\ell}$ is* sufficiently *fine, in the sense that it provides a good representation of the boundary of Ω, then* `STOP`*. Otherwise, set $\ell = \ell + 1$, and* `GOTO` *2.*

Remark 3.2. *Mesh smoothing is undertaken to ensure that the resulting mesh $\hat{\mathcal{T}}_{h_i}$, $i = 1, 2, \ldots, \ell$, is 1–irregular. We remark that additional refinement may also be undertaken to ensure that so-called islands of unrefined elements are subsequently refined, for example. In particular, near the boundary, we ensure that the elements are conforming in order to allow for subsequent movement to the boundary, cf. below.*

Remark 3.3. *The termination condition in Algorithm 3.1 should be sufficient to guarantee that nodes close to the boundary of Ω may be moved onto $\partial\Omega$ without destroying the logical connectivity of the finest reference mesh $\hat{\mathcal{T}}_{h_\ell}$, while, at the same time, not distorting the elements too much, cf. below. For example, for each $\hat{\kappa} \in \hat{\mathcal{T}}_{h_\ell}$ satisfying $\hat{\kappa} \cap \partial\Omega \neq \emptyset$, we require that for each vertex $\hat{x}_v$ of $\hat{\kappa}$, we have that $dist(\hat{x}_v, \partial\Omega) \ll h_{\hat{\kappa}}$, where $h_{\hat{\kappa}}$ denotes the granularity of $\hat{\kappa}$.*

Remark 3.4. *Algorithm 3.1 simply provides a prototype of a typical refinement algorithm that could be employed to generate the sequence of nested reference meshes $\{\hat{\mathcal{T}}_{h_i}\}_{i=1}^{\ell}$; we stress that alternative sequences of grids may also be employed.*

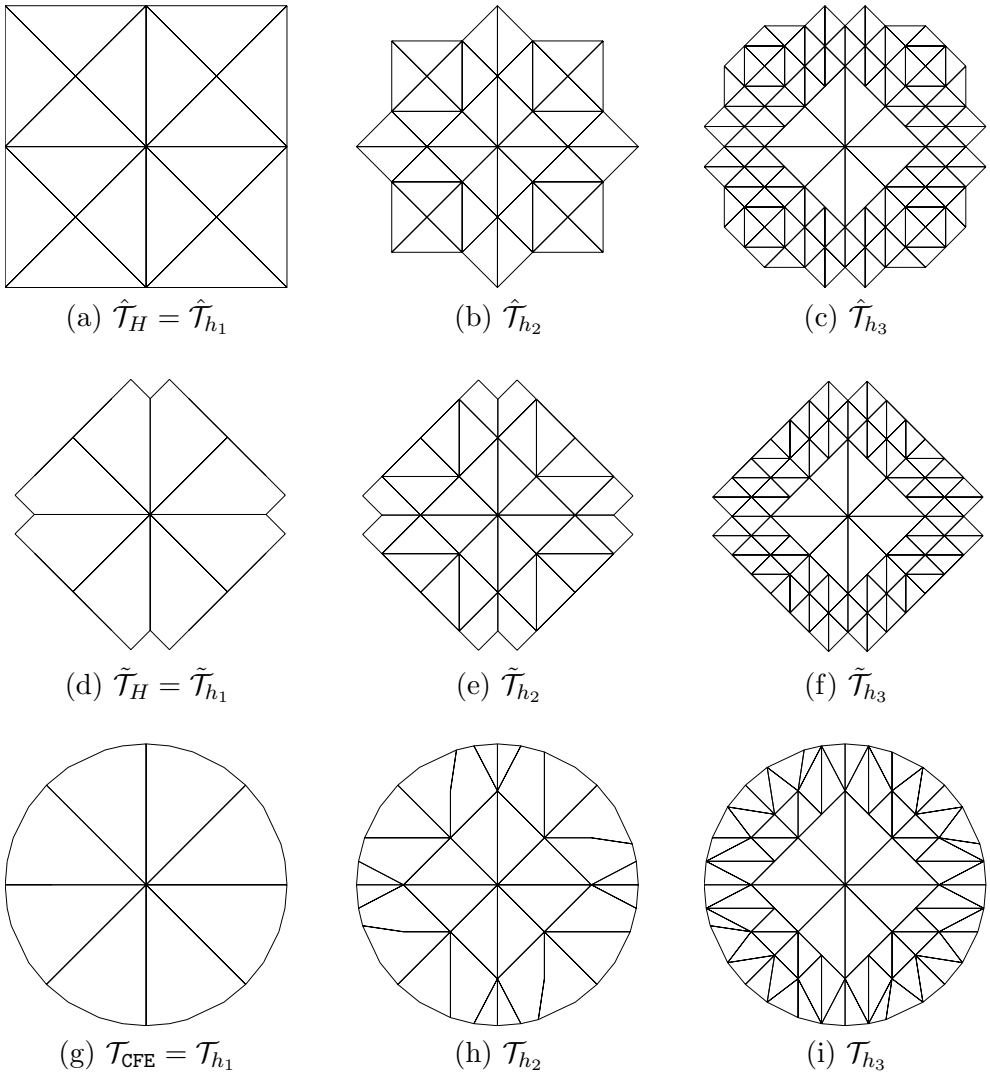

(a) $\hat{\mathcal{T}}_H = \hat{\mathcal{T}}_{h_1}$ (b) $\hat{\mathcal{T}}_{h_2}$ (c) $\hat{\mathcal{T}}_{h_3}$

(d) $\tilde{\mathcal{T}}_H = \tilde{\mathcal{T}}_{h_1}$ (e) $\tilde{\mathcal{T}}_{h_2}$ (f) $\tilde{\mathcal{T}}_{h_3}$

(g) $\mathcal{T}_{\texttt{CFE}} = \mathcal{T}_{h_1}$ (h) $\mathcal{T}_{h_2}$ (i) $\mathcal{T}_{h_3}$

Figure 1: Hierarchy of meshes: (a)–(c) Reference meshes; (d)–(f) Logical Meshes; (g)–(i) Corresponding physical meshes.

As an example, we consider the situation when Ω is a circular domain in $\mathbb{R}^2$, with center at the origin and radius 3/4. The sequence of reference grids $\{\hat{\mathcal{T}}_{h_i}\}_{i=1}^{\ell}$, generated by Algorithm 3.1, in the case when $\ell = 3$, are depicted in Figures 1(a)–(c).

We recall that the reference meshes $\{\hat{\mathcal{T}}_{h_i}\}_{i=1}^{\ell}$ are nested, cf. above. Formally, we write this as follows: given $\hat{\kappa}_i \in \hat{\mathcal{T}}_{h_i}$, for some i, where $2 \leq i \leq \ell$, the father element $\hat{\kappa}_{i-1} \in \hat{\mathcal{T}}_{h_{i-1}}$ such that $\hat{\kappa}_i \subset \hat{\kappa}_{i-1}$ is given by the mapping

$$\mathfrak{F}_{i-1}^{i}(\hat{\kappa}_i) = \hat{\kappa}_{i-1}.$$

Thereby, the mapping

$$\mathfrak{F}_{i}^{\ell} = \mathfrak{F}_{i}^{i+1} \circ \mathfrak{F}_{i+1}^{i+2} \circ \ldots \circ \mathfrak{F}_{\ell-1}^{\ell},$$

provides the link between the father elements on the reference mesh $\hat{\mathcal{T}}_{h_i}$, $i = 1, \ldots, \ell-1$, with its children on the finest reference mesh $\hat{\mathcal{T}}_{h_\ell}$. More precisely, given an element $\hat{\kappa}_\ell \in \hat{\mathcal{T}}_{h_\ell}$, the father element $\hat{\kappa}_i \in \hat{\mathcal{T}}_{h_i}$, $i = 1, \ldots, \ell-1$, which satisfies $\hat{\kappa}_\ell \subset \hat{\kappa}_i$ is given by:

$$\mathfrak{F}_{i}^{\ell}(\hat{\kappa}_\ell) = \hat{\kappa}_i.$$

We now proceed to define the sequence of logical and physical meshes $\tilde{\mathcal{T}}_{h_i}$ and $\mathcal{T}_{h_i}$, $i = 1, \ldots, \ell$, respectively. To this end, we write $\hat{\mathcal{N}}_i$ to denote the set of nodal (mesh) points which define the reference mesh $\hat{\mathcal{T}}_{h_i}$, $i = 1, \ldots, \ell$, respectively. The finest physical mesh $\mathcal{T}_{h_\ell}$ is defined from the reference mesh $\hat{\mathcal{T}}_{h_\ell}$ by moving grid points $\hat{x} \in \hat{\mathcal{N}}_\ell$ of $\hat{\mathcal{T}}_{h_\ell}$ which are close to the boundary $\partial\Omega$, i.e., points which satisfy $\text{dist}(\hat{x}, \partial\Omega) \ll h_{\hat{\kappa}}$, for example. During this process some elements of the reference mesh $\hat{\mathcal{T}}_{h_\ell}$ may end up lying completely outside the computational domain; in this case, they are removed from the physical mesh $\mathcal{T}_{h_\ell}$. More precisely, the process of moving nodes $\hat{x} \in \hat{\mathcal{N}}_\ell$ onto the boundary naturally defines the bijective mapping

$$\Phi : \hat{\mathcal{N}}_\ell \to \mathcal{N}_\ell,$$

where $\mathcal{N}_\ell$ denotes the set of mapped vertex points.

With this construction, the mapping Φ can be employed to map an element $\hat{\kappa} \in \hat{\mathcal{T}}_{h_\ell}$ to a so–called physical element κ. To simplify notation, we simply refer to this mapping as Φ as well; thereby, we write

$$\Phi(\hat{\kappa}) = \kappa.$$

In this setting, Φ is bijective relative to the elements which are not removed from the mesh under refinement. During the process of moving nodes onto the boundary $\partial\Omega$, we noted that some elements in the reference mesh $\hat{\mathcal{T}}_{h_\ell}$ may be removed. With this in mind we define the finest *logical mesh* $\tilde{\mathcal{T}}_{h_\ell}$ to be equal to the set of elements in the reference mesh $\hat{\mathcal{T}}_{h_\ell}$ which are needed to construct the finest physical mesh $\mathcal{T}_{h_\ell}$. Thereby, $\tilde{\mathcal{T}}_{h_\ell} \subseteq \hat{\mathcal{T}}_{h_\ell}$; indeed, in the case when $\Phi \equiv I$ (the identity operator), then clearly $\tilde{\mathcal{T}}_{h_\ell} = \hat{\mathcal{T}}_{h_\ell}$. Given that any element $\tilde{\kappa} \in \tilde{\mathcal{T}}_{h_\ell}$ also satisfies $\tilde{\kappa} \in \hat{\mathcal{T}}_{h_\ell}$, we note that

$$\Phi(\tilde{\kappa}) = \kappa,$$

for some $\kappa \in \mathcal{T}_{h_\ell}$.

With this notation the physical fine mesh $\mathcal{T}_{h_\ell}$ may be defined as follows:

$$\mathcal{T}_{h_\ell} = \{\kappa : \kappa = \Phi(\tilde{\kappa}) \ \text{ for some } \ \tilde{\kappa} \in \tilde{\mathcal{T}}_{h_\ell}\}.$$

The newly created finest physical mesh $\mathcal{T}_{h_\ell}$ is a *standard* boundary conforming mesh upon which standard finite element/finite volume methods may be applied. In the current context,

we assume that the geometry is *complicated* in the sense that $\mathcal{T}_{h_\ell}$ is too fine to undertake computations. Instead, we wish to only use $\mathcal{T}_{h_\ell}$ to create a coarse composite finite element mesh $\mathcal{T}_{\texttt{CFE}}$ upon which numerical simulations will be performed.

With this construction, we may now naturally create a hierarchy of logical and physical meshes $\{\tilde{\mathcal{T}}_{h_i}\}_{i=1}^{\ell}$ and $\{\mathcal{T}_{h_i}\}_{i=1}^{\ell}$, respectively, by simply coarsening $\tilde{\mathcal{T}}_{h_\ell}$ and $\mathcal{T}_{h_\ell}$, respectively. In order to ensure that these meshes are nested, the element domains within these meshes may consist of general polygons; this is in contrast to the construction outlined in [11] where sequences of non-nested meshes consisting of standard element types are defined. To this end, we write

$$\begin{aligned}
\tilde{\mathcal{T}}_{h_i} &= \{\tilde{\kappa} : \tilde{\kappa} = \cup\tilde{\kappa}_\ell,\ \tilde{\kappa}_\ell \in \tilde{\mathcal{T}}_{h_\ell},\ \text{ which share a common parent from mesh level } i, \text{ i.e.,} \\
&\qquad \mathfrak{F}_i^\ell(\tilde{\kappa}_\ell)\ \text{ is the same for all members of this set}\}, \\
\mathcal{T}_{h_i} &= \{\kappa : \kappa = \cup\kappa_\ell,\ \kappa_\ell \in \mathcal{T}_{h_\ell},\ \text{ which share a common parent from mesh level } i, \text{ i.e.,} \\
&\qquad \mathfrak{F}_i^\ell(\Phi^{-1}(\kappa_\ell))\ \text{ is the same for all members of this set}\},
\end{aligned}$$

$i = 1, \ldots, \ell - 1$. Returning to the above example, when Ω is a circular domain in $\mathbb{R}^2$, the sequence of logical and physical grids $\{\tilde{\mathcal{T}}_{h_i}\}_{i=1}^{\ell}$ and $\{\mathcal{T}_{h_i}\}_{i=1}^{\ell}$, respectively, in the case when $\ell = 3$, are depicted in Figures 1(d)–(f) and Figures 1(g)–(i), respectively. We refer to the coarsest level physical mesh $\mathcal{T}_{h_1}$ to as the *composite finite element mesh*; in particular, we denote this by $\mathcal{T}_{\texttt{CFE}}$, i.e., $\mathcal{T}_{\texttt{CFE}} = \mathcal{T}_{h_1}$.

With this notation the mapping Φ may be employed to transform an element $\kappa \in \mathcal{T}_{\texttt{CFE}}$ to the corresponding element $\tilde{\kappa} \in \mathcal{T}_{h_1}$; here, we denote the restriction of Φ to κ by Φ_κ such that $\Phi_\kappa(\tilde{\kappa}) = \kappa$. Since only nodes close to the boundary are moved, we assume that the element mapping Φ_κ defines the shape of κ, without any significant rescaling. With this in mind, we assume that the element mapping Φ_κ is close to the identity in the following sense: the Jacobi matrix J_{Φ_κ} of Φ_κ satisfies

$$C_1^{-1} \leq \|\det J_{\Phi_\kappa}\|_{L_\infty(\kappa)} \leq C_1, \quad \|J_{\Phi_\kappa}^{-\top}\|_{L_\infty(\kappa)} \leq C_2, \quad \|J_{\Phi_\kappa}^{-\top}\|_{L_\infty(\partial\kappa)} \leq C_3 \tag{3}$$

for all κ in $\mathcal{T}_{\texttt{CFE}}$ uniformly throughout the mesh for some positive constants C_1, C_2, and C_3. This will be important as our error estimates will be expressed in terms of Sobolev norms over the element domains $\tilde{\kappa}$.

3.2 Finite element spaces

Corresponding to the meshes $\{\mathcal{T}_{h_i}\}_{i=1}^{\ell}$, we define the corresponding sequence of discontinuous Galerkin (DG) finite element spaces $V(\mathcal{T}_{h_i}, p)$, $i = 1, \ldots, \ell$, respectively, consisting of piecewise discontinuous polynomials of degree p. For simplicity of presentation, we first assume that the polynomial degree is uniformly distributed over the mesh $\mathcal{T}_{h_\ell}$; the extension to variable polynomial degrees follows in a natural fashion, cf. below. With this in mind, we write

$$V(\mathcal{T}_{h_i}, p) = \{u \in L_2(\Omega) : u|_\kappa \in \mathcal{P}_p(\kappa)\ \forall \kappa \in \mathcal{T}_{h_i}\},$$

$i = 1, \ldots, \ell$, where $\mathcal{P}_p(\kappa)$ denotes the set of polynomials of degree at most $p \geq 1$ defined over the general polygon κ.

With this construction, noting that the meshes $\{\mathcal{T}_{h_i}\}_{i=1}^{\ell}$ are nested, we deduce that

$$V(\mathcal{T}_{h_1}, p) \subset V(\mathcal{T}_{h_2}, p) \subset \ldots \subset V(\mathcal{T}_{h_\ell}, p).$$

The classical prolongation (injection) operator from $V(\mathcal{T}_{h_i}, p)$ to $V(\mathcal{T}_{h_{i+1}}, p)$, $1 \leq i \leq \ell - 1$ is denoted by

$$P_i^{i+1} : V(\mathcal{T}_{h_i}, p) \to V(\mathcal{T}_{h_{i+1}}, p), \quad i = 1, \ldots, \ell - 1.$$

Thereby, we may define the prolongation operator from $V(\mathcal{T}_{h_i}, p)$ to $V(\mathcal{T}_{h_\ell}, p)$, $1 \leq i \leq \ell - 1$, by

$$P_i = P_{\ell-1}^{\ell} P_{\ell-2}^{\ell-1} \ldots P_i^{i+1}.$$

With this notation, we may write $V(\mathcal{T}_{h_i}, p)$, $1 \leq i \leq \ell - 1$, in the following alternative form

$$V(\mathcal{T}_{h_i}, p) = \{u \in L_2(\Omega) : u = P_i^{\top} \phi,\ \phi \in V(\mathcal{T}_{h_\ell}, p)\}, \tag{4}$$

where the restriction operator $P_i^{\top}$ is defined as the transpose of P_i.

Remark 3.5. *The use of the prolongation operator P_i within the definition of the finite element spaces $V(\mathcal{T}_{h_i}, p)$, $i = 1, \ldots, \ell$, given in (4) allows for the introduction of different spaces, depending on the specific choice of P_i. Indeed, here the finite element spaces are constructed in such a manner that on each (composite) element $\kappa \in \mathcal{T}_{h_i}$, $i = 1, \ldots, \ell$, a the restriction of a function $v \in V(\mathcal{T}_{h_i}, p)$ to κ is a polynomial of degree p. This is in contrast to the construction considered in [11]; indeed, [11] employs basis functions which are* piecewise *polynomials on each composite element domain. Note also, that [11] employs finite element spaces consisting of continuous, rather than discontinuous, piecewise polynomials.*

We now refer to $V(\mathcal{T}_{h_1}, p)$ as the composite finite element space $V(\mathcal{T}_{\mathtt{CFE}}, p)$, i.e., $V(\mathcal{T}_{\mathtt{CFE}}, p) = V(\mathcal{T}_{h_1}, p)$. The use of a variable polynomial degree on each composite element $\kappa \in \mathcal{T}_{\mathtt{CFE}}$ may now be admitted in a natural fashion. Indeed, writing $\boldsymbol{p}$ to denote the composite polynomial degree vector, such that $\boldsymbol{p}|_\kappa = p_\kappa$, we define the corresponding composite finite element space $V(\mathcal{T}_{\mathtt{CFE}}, \boldsymbol{p})$. In this setting, it is implicitly assumed that the children of the element $\kappa \in \mathcal{T}_{\mathtt{CFE}}$ all have the same polynomial degree p_κ.

4 Composite discontinuous Galerkin finite element method

In this section, we introduce the *hp*-version of the (symmetric) interior penalty DGCFEM for the numerical approximation of (1)–(2). To this end, we first introduce the following notation.

We denote by $\mathcal{F}_{\mathtt{CFE}}^{\mathcal{I}}$ the set of all interior faces of the partition $\mathcal{T}_{\mathtt{CFE}}$ of Ω, and by $\mathcal{F}_{\mathtt{CFE}}^{\mathcal{B}}$ the set of all boundary faces of $\mathcal{T}_{\mathtt{CFE}}$. Furthermore, we define $\mathcal{F} = \mathcal{F}_{\mathtt{CFE}}^{\mathcal{I}} \cup \mathcal{F}_{\mathtt{CFE}}^{\mathcal{B}}$. The boundary $\partial\kappa$ of an element κ and the sets $\partial\kappa \setminus \partial\Omega$ and $\partial\kappa \cap \partial\Omega$ will be identified in a natural way with the corresponding subsets of $\mathcal{F}$. Let κ^+ and κ^- be two adjacent elements of $\mathcal{T}_{\mathtt{CFE}}$, and $\mathbf{x}$ an arbitrary point on the interior face $F \in \mathcal{F}_{\mathtt{CFE}}^{\mathcal{I}}$ given by $F = \partial\kappa^+ \cap \partial\kappa^-$. Furthermore, let v and $\mathbf{q}$ be scalar- and vector-valued functions, respectively, that are smooth inside each element $\kappa^\pm$. By $(v^\pm, \mathbf{q}^\pm)$, we denote the traces of $(v, \mathbf{q})$ on F taken from within the interior of $\kappa^\pm$, respectively. Then, the averages of v and $\mathbf{q}$ at $\mathbf{x} \in F$ are given by

$$\{\!\{v\}\!\} = \frac{1}{2}(v^+ + v^-), \qquad \{\!\{\mathbf{q}\}\!\} = \frac{1}{2}(\mathbf{q}^+ + \mathbf{q}^-),$$

respectively. Similarly, the jumps of v and $\mathbf{q}$ at $\mathbf{x} \in F$ are given by

$$[\![v]\!] = v^+ \, \mathbf{n}_{\kappa^+} + v^- \, \mathbf{n}_{\kappa^-}, \qquad [\![\mathbf{q}]\!] = \mathbf{q}^+ \cdot \mathbf{n}_{\kappa^+} + \mathbf{q}^- \cdot \mathbf{n}_{\kappa^-},$$

respectively, where we denote by $\mathbf{n}_{\kappa^\pm}$ the unit outward normal vector of $\partial\kappa^\pm$, respectively. On a boundary face $F \in \mathcal{F}^{\mathcal{B}}_{\mathtt{CFE}}$, we set $\{\!\{v\}\!\} = v$, $\{\!\{\mathbf{q}\}\!\} = \mathbf{q}$, and $[\![v]\!] = v\mathbf{n}$, with $\mathbf{n}$ denoting the unit outward normal vector on the boundary $\partial\Omega$.

With this notation, we make the following key assumptions:

(A1) For all elements $\kappa \in \mathcal{T}_{\mathtt{CFE}}$, we define

$$C_\kappa = \mathrm{card}\left\{F \in \mathcal{F}^{\mathcal{I}}_{\mathtt{CFE}} \cup \mathcal{F}^{\mathcal{B}}_{\mathtt{CFE}} : F \subset \partial\kappa\right\}.$$

In the following we assume that there exists a positive constant C_F such that

$$\max_{\kappa\in\mathcal{T}_{\mathtt{CFE}}} C_\kappa \leq C_F,$$

uniformly with respect to the mesh size.

(A2) Inverse inequality. Given a face $F \in \mathcal{F}^{\mathcal{I}}_{\mathtt{CFE}} \cup \mathcal{F}^{\mathcal{B}}_{\mathtt{CFE}}$ of an element $\kappa \in \mathcal{T}_{\mathtt{CFE}}$, there exists a positive constant C_{inv}, independent of the local mesh size and local polynomial order, such that

$$\|\nabla v\|^2_{L_2(F)} \leq C_{\mathrm{inv}} \frac{p^2_\kappa}{h_F} \|\nabla v\|^2_{L_2(\kappa)}$$

for all $v \in V(\mathcal{T}_{\mathtt{CFE}}, \boldsymbol{p})$, where h_F is a *representative* length scale associated to the face $F \subset \partial\kappa$.

(A3) We assume that the polynomial degree vector $\boldsymbol{p}$ is of bounded local variation, that is, there is a constant $\rho \geq 1$ such that

$$\rho^{-1} \leq p_\kappa / p_{\kappa'} \leq \rho,$$

whenever κ and κ' share a common face ($(d-1)$–dimensional facet).

Remark 4.1. *We remark that in the case when κ is a 'standard' (isotropic) element in the sense that $\kappa = \hat{\kappa} \in \hat{\mathcal{T}}_H$, for example, the inverse inequality stated in Assumption (A2) immediately follows from [9, 4], for example, with $h_F = h_\kappa$. Moreover, [9] also considers the case when the underlying mesh consists of anisotropic elements; loosely speaking, in this latter setting, h_F must be chosen to be the dimension of the element κ in the orthogonal direction to the face F under consideration. For general composite elements, which intersect the boundary of the computational domain, the above inverse inequality is expected to hold with $h_F \approx h_\ell$, where $h_\ell \approx h_\kappa / 2^{\ell-1}$.*

With this notation, we consider the (symmetric) interior penalty DGCFEM for the numerical approximation of (1)–(2): find $u_h \in V(\mathcal{T}_{\mathtt{CFE}}, \boldsymbol{p})$ such that

$$B_{\mathtt{DG}}(u_h, v) = F_h(v) \tag{5}$$

for all $v \in V(\mathcal{T}_{\mathtt{CFE}}, \boldsymbol{p})$, where

$$\begin{aligned} B_{\mathtt{DG}}(u,v) = &\sum_{\kappa\in\mathcal{T}_{\mathtt{CFE}}} \int_\kappa \nabla u \cdot \nabla v \, d\mathbf{x} - \sum_{F\in\mathcal{F}^{\mathcal{I}}_{\mathtt{CFE}}\cup\mathcal{F}^{\mathcal{B}}_{\mathtt{CFE}}} \int_F \left(\{\!\{\nabla_h v\}\!\} \cdot [\![u]\!] + \{\!\{\nabla_h u\}\!\} \cdot [\![v]\!]\right) ds \\ &+ \sum_{F\in\mathcal{F}^{\mathcal{I}}_{\mathtt{CFE}}\cup\mathcal{F}^{\mathcal{B}}_{\mathtt{CFE}}} \int_F \sigma \, [\![u]\!] \cdot [\![v]\!] \, ds, \\ F_h(v) = &\int_\Omega f v \, d\mathbf{x}. \end{aligned}$$

Here, ∇_h denotes the elementwise gradient operator. Furthermore, the function $\sigma \in L^\infty(\mathcal{F}^{\mathcal{I}}_{\mathtt{CFE}} \cup \mathcal{F}^{\mathcal{B}}_{\mathtt{CFE}})$ is the discontinuity stabilization function that is chosen as follows: we define the function $\mathtt{p} \in L^\infty(\mathcal{F}^{\mathcal{I}}_{\mathtt{CFE}} \cup \mathcal{F}^{\mathcal{B}}_{\mathtt{CFE}})$ by

$$\mathtt{p}(\mathbf{x}) := \begin{cases} \max(p_\kappa, p_{\kappa'}), & \mathbf{x} \in F \in \mathcal{F}^{\mathcal{I}}_{\mathtt{CFE}},\ F = \partial\kappa \cap \partial\kappa', \\ p_\kappa, & \mathbf{x} \in F \in \mathcal{F}^{\mathcal{B}}_{\mathtt{CFE}},\ F \in \partial\kappa \cap \partial\Omega, \end{cases}$$

and set

$$\sigma|_F = \gamma \mathtt{p}^2 h_F^{-1}, \tag{6}$$

with a parameter $\gamma > 0$ that is independent of h_F and $\mathbf{p}$.

5 Stability analysis

Before embarking on the error analysis of the *hp*–version DGCFEM (5), we first derive some preliminary results. Let us first introduce the DG–norm $|||\cdot|||_{\mathtt{DG}}$ by

$$|||\, v \,|||^2_{\mathtt{DG}} \;=\; \sum_{\kappa \in \mathcal{T}_{\mathtt{CFE}}} \|\nabla v\|^2_{L_2(\kappa)} + \sum_{F \in \mathcal{F}^{\mathcal{I}}_{\mathtt{CFE}} \cup \mathcal{F}^{\mathcal{B}}_{\mathtt{CFE}}} \|\sigma^{1/2} [\![v]\!]\|^2_{L_2(F)}. \tag{7}$$

For a given face $F \in \mathcal{F}^{\mathcal{I}}_{\mathtt{CFE}} \cup \mathcal{F}^{\mathcal{B}}_{\mathtt{CFE}}$, such that $F \subset \partial\kappa$ for some $\kappa \in \mathcal{T}_{\mathtt{CFE}}$, we write $\tilde{F}$ to denote the respective face of the mapped element $\tilde{\kappa}$ based on employing the element mapping Φ_κ. More precisely, we write $\tilde{F} = \Phi_\kappa^{-1}(F)$. Further, we define m_F and $m_{\tilde{F}}$ to denote the $(d-1)$–dimensional measure (volume) of the faces F and $\tilde{F}$, respectively. In view of (3), we note that there exists a positive constant C_4, such that

$$C_4^{-1} m_{\tilde{F}} \leq m_F \leq C_4 m_{\tilde{F}} \tag{8}$$

for every face $F \in \mathcal{F}^{\mathcal{I}}_{\mathtt{CFE}} \cup \mathcal{F}^{\mathcal{B}}_{\mathtt{CFE}}$. Moreover, the surface Jacobian $S_{F,\tilde{F}}$ arising in the transformation of the face F to $\tilde{F}$ may be uniformly bounded in the following manner

$$\|S_{F,\tilde{F}}\|_{L_\infty(\tilde{F})} \leq C_5 \tag{9}$$

for all faces $F \in \mathcal{F}^{\mathcal{I}}_{\mathtt{CFE}} \cup \mathcal{F}^{\mathcal{B}}_{\mathtt{CFE}}$, where C_5 is a positive constant.

Lemma 5.1. *With σ defined as in (6), there exists a positive constant C, which depends only on the constants C_F and C_{inv}, cf. Assumptions (A1) , (A2) and (A3) above, respectively, such that*

$$B_{\mathtt{DG}}(v,v) \geq C |||\, v \,|||^2_{\mathtt{DG}} \quad \forall v \in V(\mathcal{T}_{\mathtt{CFE}}, \boldsymbol{p}), \tag{10}$$

provided that the (positive) constant γ arising in the definition of the discontinuity penalization parameter σ is chosen sufficiently large.

Proof. For $v \in V(\mathcal{T}_{\mathtt{CFE}}, \boldsymbol{p})$, we note that

$$\begin{aligned} B_{\mathtt{DG}}(v,v) \;&=\; \sum_{\kappa \in \mathcal{T}_{\mathtt{CFE}}} \|\nabla v\|^2_{L_2(\kappa)} - 2 \sum_{F \in \mathcal{F}^{\mathcal{I}}_{\mathtt{CFE}} \cup \mathcal{F}^{\mathcal{B}}_{\mathtt{CFE}}} \int_F \{\!\{ \nabla v \}\!\} \cdot [\![v]\!] \, \mathrm{d}s + \sum_{F \in \mathcal{F}^{\mathcal{I}}_{\mathtt{CFE}} \cup \mathcal{F}^{\mathcal{B}}_{\mathtt{CFE}}} \|\sigma^{1/2} [\![v]\!]\|^2_{L_2(F)}, \\ &\equiv\; \mathrm{I} + \mathrm{II} + \mathrm{III}. \end{aligned} \tag{11}$$

In order to bound term II, we first note that for $F \in \mathcal{F}^{\mathcal{I}}_{\mathtt{CFE}}$, we have that

$$\begin{aligned}\int_F \{\!\{\nabla v\}\!\} \cdot [\![v]\!] \,\mathrm{d}s &\leq \|\sigma^{-1/2}\{\!\{\nabla v\}\!\}\|_{L_2(F)}\|\sigma^{1/2}[\![v]\!]\|_{L_2(F)} \\ &\leq \frac{1}{2}\left(\|\sigma^{-1/2}\nabla v^+\|_{L_2(F)} + \|\sigma^{-1/2}\nabla v^-\|_{L_2(F)}\right)\|\sigma^{1/2}[\![v]\!]\|_{L_2(F)} \\ &\leq \epsilon\left(\|\sigma^{-1/2}\nabla v^+\|^2_{L_2(F)} + \|\sigma^{-1/2}\nabla v^-\|^2_{L_2(F)}\right) + \frac{1}{8\epsilon}\|\sigma^{1/2}[\![v]\!]\|^2_{L_2(F)};\end{aligned}$$

here, we have employed the Cauchy–Schwarz inequality, together with the arithmetic–geometric mean inequality. Employing the inverse inequality stated in Assumption (A2), together with (A3), we deduce that

$$\begin{aligned}\int_F \{\!\{\nabla v\}\!\} \cdot [\![v]\!] \,\mathrm{d}s &\leq C_{\mathrm{inv}}\epsilon\left(\frac{p^2_{\kappa^+}}{h_F}\|\sigma^{-1/2}\nabla v\|^2_{L_2(\kappa^+)} + \frac{p^2_{\kappa^-}}{h_F}\|\sigma^{-1/2}\nabla v\|^2_{L_2(\kappa^-)}\right) \\ &\quad + \frac{1}{8\epsilon}\|\sigma^{1/2}[\![v]\!]\|^2_{L_2(F)} \\ &\leq \frac{C_{\mathrm{inv}}\rho^2}{\gamma}\epsilon\left(\|\nabla v\|^2_{L_2(\kappa^+)} + \|\nabla v\|^2_{L_2(\kappa^-)}\right) + \frac{1}{8\epsilon}\|\sigma^{1/2}[\![v]\!]\|^2_{L_2(F)}, \qquad (12)\end{aligned}$$

where we have used the definition of the interior penalty parameter σ, cf. (6).

In an analogous fashion, for $F \in \mathcal{F}^{\mathcal{B}}_{\mathtt{CFE}}$, we have that

$$\int_F \{\!\{\nabla v\}\!\} \cdot [\![v]\!] \,\mathrm{d}s \leq \frac{C_{\mathrm{inv}}}{\gamma}\epsilon\|\nabla v\|^2_{L_2(\kappa^+)} + \frac{1}{4\epsilon}\|\sigma^{1/2}[\![v]\!]\|^2_{L_2(F)}. \qquad (13)$$

Thereby, exploiting Assumption (A1) above, inserting (12) and (13) into (11) gives

$$B_{\mathtt{DG}}(v,v) = \left(1 - \frac{C_{\mathrm{inv}}C_F\rho^2}{\gamma}\epsilon\right)\sum_{\kappa\in\mathcal{T}_{\mathtt{CFE}}}\|\nabla v\|^2_{L_2(\kappa)} + \left(1 - \frac{1}{4\epsilon}\right)\sum_{F\in\mathcal{F}^{\mathcal{I}}_{\mathtt{CFE}}\cup\mathcal{F}^{\mathcal{B}}_{\mathtt{CFE}}}\|\sigma^{1/2}[\![v]\!]\|^2_{L_2(F)}.$$

Thereby, the bilinear form $B_{\mathtt{DG}}(\cdot,\cdot)$ is coercive over $V(\mathcal{T}_{\mathtt{CFE}},\boldsymbol{p}) \times V(\mathcal{T}_{\mathtt{CFE}},\boldsymbol{p})$, assuming that $\epsilon > 1/4$ and $\gamma > C_{\mathrm{inv}}C_F\rho^2\epsilon$. □

6 Approximation results

In this section we develop the approximation results needed for the forthcoming *a priori* error estimation developed in Section 7. To this end, given $\kappa \in \mathcal{T}_{\mathtt{CFE}}$, we write $\tilde{\kappa} \in \tilde{\mathcal{T}}_{h_1}$ to denote the corresponding element from the logical mesh $\tilde{\mathcal{T}}_{h_1}$ which satisfies $\Phi(\tilde{\kappa}) = \kappa$. Moreover, we write $\hat{\kappa} \in \hat{\mathcal{T}}_{h_1}$ to denote the element in the reference mesh $\hat{\mathcal{T}}_{h_1}$ such that $\tilde{\kappa} \subseteq \hat{\kappa}$.

With this notation, we now recall the following approximation result.

Lemma 6.1. *Suppose that $\hat{\kappa} \in \hat{\mathcal{T}}_{h_1}$ is a d–simplex or d–parallelepiped of diameter $h_{\hat{\kappa}}$. Suppose further that $v|_{\hat{\kappa}} \in H^{k_{\hat{\kappa}}}(\hat{\kappa})$, $k_{\hat{\kappa}} \geq 0$, for $\hat{\kappa} \in \hat{\mathcal{T}}_{h_1}$. Then, there exists $\hat{\Pi}_p v$ in $\mathcal{P}_{p_{\hat{\kappa}}}(\hat{\kappa})$, $p_{\hat{\kappa}} = 1, 2, \ldots,$ such that for $0 \leq m \leq k_{\hat{\kappa}}$,*

$$\|v - \hat{\Pi}_p v\|_{H^m(\hat{\kappa})} \leq C\frac{h^{s_{\hat{\kappa}}-m}_{\hat{\kappa}}}{p^{k_{\hat{\kappa}}-q}_{\hat{\kappa}}}\|v\|_{H^{k_{\hat{\kappa}}}(\hat{\kappa})},$$

where $1 \leq s_{\hat{\kappa}} \leq \min\{p_{\hat{\kappa}}+1, k_{\hat{\kappa}}\}$, $p_{\hat{\kappa}} \geq 1$, for $\hat{\kappa} \in \hat{\mathcal{T}}_{h_1}$, and C is a positive constant, independent of v and the discretisation parameters.

Proof. For the proof, see Lemma 4.5 in [5] for $d = 2$; when $d > 2$ the argument is completely analogous. □

Given the operator $\hat{\Pi}_p$ defined in Lemma 6.1, we define the projection operators $\tilde{\Pi}_p$ and Π_p on $\tilde{\kappa}$ and κ, respectively, by the relations

$$\tilde{\Pi}_p \tilde{v} = \hat{\Pi}_p(\mathfrak{E}\tilde{v})|_{\tilde{\kappa}}, \qquad \Pi_p v = (\tilde{\Pi}_p(v \circ \Phi)) \circ \Phi^{-1},$$

where $\mathfrak{E}$ denotes the extension operator defined in Theorem 2.1. With this notation, we state the following approximation result.

Lemma 6.2. *Given $\kappa \in \mathcal{T}_{\mathtt{CFE}}$, let $F \subset \partial\kappa$ denote one of its faces. For a function $v \in H^{k_\kappa}(\kappa)$, the following bounds hold*

$$|v - \Pi_p v|_{H^m(\kappa)} \leq C \frac{h_\kappa^{s_\kappa - m}}{p_\kappa^{k_\kappa - m}} \|\mathfrak{E}\tilde{v}\|_{H^{k_\kappa}(\hat{\kappa})}, \tag{14}$$

$$|v - \Pi_p v|_{H^m(F)} \leq C \frac{1}{h_F^{1/2}} \frac{h_\kappa^{s_\kappa - m}}{p_\kappa^{k_\kappa - m - 1/2}} \|\mathfrak{E}\tilde{v}\|_{H^{k_\kappa}(\hat{\kappa})}, \tag{15}$$

where $0 \leq m \leq k_\kappa$, $1 \leq s_\kappa \leq \min\{p_\kappa + 1, k_\kappa\}$, $p_\kappa \geq 1$, and C is a positive constant, independent of v and the discretisation parameters.

Proof. The proof is based on exploiting a scaling argument together with (3) and Lemma 6.1. To this end, we have

$$\begin{aligned} |v - \Pi_p v|^2_{H^m(\kappa)} &\leq \|\det J_{\Phi_\kappa}\|_{L_\infty(\kappa)} \|J_{\Phi_\kappa}^{-\top}\|^{2m}_{L_\infty(\kappa)} |\tilde{v} - \tilde{\Pi}_p \tilde{v}|^2_{H^m(\tilde{\kappa})} \\ &\leq C_1 (C_2)^{2m} |\mathfrak{E}\tilde{v} - \hat{\Pi}_p(\mathfrak{E}\tilde{v})|^2_{H^m(\hat{\kappa})} \\ &\leq C \frac{h_\kappa^{2(s_\kappa - m)}}{p_\kappa^{2(k_\kappa - m)}} \|\mathfrak{E}\tilde{v}\|^2_{H^{k_\kappa}(\hat{\kappa})}, \end{aligned} \tag{16}$$

which gives (14). To prove (15), we first recall the multiplicative trace inequality

$$\|v\|^2_{L_2(F)} \leq C(\|\nabla v\|_{L_2(\kappa)} \|v\|_{L_2(\kappa)} + h_F^{-1} \|v\|^2_{L_2(\kappa)}), \tag{17}$$

where C is a positive independent of the meshsize. We remark, cf. Remark 4.1, that h_F appears in (17) rather than h_κ due to the general shape of the element κ. Employing (17), together with (3), (9), (8) and (14) we immediately deduce (15). □

7 A priori error analysis

In this section we derive an *a priori* error bound for the interior penalty DGCFEM introduced in Section 4. To this end, we decompose the global error $u - u_h$ as

$$u - u_h = (u - \Pi_p u) + (\Pi_p u - u_h) \equiv \eta + \xi\,, \tag{18}$$

where Π_p denotes the projection operator introduced in Section 6. With these definitions we have the following result.

Lemma 7.1. *For $u \in H^{3/2+\epsilon}(\Omega)$, $\epsilon > 0$, the functions ξ and η defined by (18) satisfy the following inequality*

$$|||\,\xi\,|||_{\mathtt{DG}} \;\leq\; C|||\,\eta\,|||^{*}_{\mathtt{DG}},$$

where

$$|||\,\eta\,|||^{*}_{\mathtt{DG}} = \left(\sum_{\kappa\in\mathcal{T}_{\mathtt{CFE}}} \|\nabla\eta\|^2_{L_2(\kappa)} + \sum_{F\in\mathcal{F}^{\mathcal{I}}_{\mathtt{CFE}}\cup\mathcal{F}^{\mathcal{B}}_{\mathtt{CFE}}} \left(\|\sigma^{-1/2}\{\!\{\nabla\eta\}\!\}\|^2_{L_2(F)} + \|\sigma^{1/2}[\![\eta]\!]\|^2_{L_2(F)}\right)\right)^{1/2}$$

and C is a positive constant that depends only on the dimension d.

Proof. This result follows from application of the Galerkin orthogonality of the DGCFEM, together with the inverse inequality in Assumption (A2); for details, see [12, 19]. □

With this result, we now proceed to prove the main result of this section.

Theorem 7.2. *Let $\Omega \subset \mathbb{R}^d$ be a bounded polyhedral domain, and let $\mathcal{T}_{\mathtt{CFE}} = \{\kappa\}$ be a subdivision of Ω as outlined in Section 3.1, where κ has diameter h_κ. Let $u_h \in V(\mathcal{T}_{\mathtt{CFE}}, p)$ be the composite discontinuous Galerkin approximation to u defined by (5) and suppose that $u|_\kappa \in H^{k_\kappa}(\kappa)$ for each $\kappa \in \mathcal{T}_{\mathtt{CFE}}$ for integers $k_\kappa \geq 1$. Then, the following error bound holds*

$$|||\,u - u_h\,|||^2_{\mathtt{DG}} \leq C \sum_{\kappa\in\mathcal{T}_{\mathtt{CFE}}} \frac{h_\kappa^{2s_\kappa}}{h_F^2}\frac{1}{p_\kappa^{2k_\kappa-3}}\|\mathfrak{E}\tilde{u}\|^2_{H^{k_\kappa}(\hat{\kappa})},$$

for any integers s_κ, $1 \leq s_\kappa \leq \min(p_\kappa+1, k_\kappa)$, and $p_\kappa \geq 1$. Here, C is a positive constant that depends only on the dimension d and the shape-regularity of $\hat{\mathcal{T}}_H$.

Proof. Decomposing the error $u - u_h$ as in (18), and exploiting Lemma 7.1, we deduce that

$$|||\,u - u_h\,|||_{\mathtt{DG}} \leq |||\,\eta\,|||_{\mathtt{DG}} + C|||\,\eta\,|||^{*}_{\mathtt{DG}} \leq (1+C)|||\,\eta\,|||^{*}_{\mathtt{DG}}. \tag{19}$$

Employing Lemma 6.2, together with the definition of the interior penalty parameter (6), we deduce that

$$|||\,\eta\,|||^{*}_{\mathtt{DG}} \leq C\left[\sum_{\kappa\in\mathcal{T}_{\mathtt{CFE}}}\left(\frac{h_\kappa^{2(s_\kappa-1)}}{p_\kappa^{2(k_\kappa-1)}} + \frac{h_\kappa^{2(s_\kappa-1)}}{p_\kappa^{2k_\kappa-1}} + \frac{h_\kappa^{2s_\kappa}}{h_F^2}\frac{1}{p_\kappa^{2k_\kappa-3}}\right)\|\mathfrak{E}\tilde{u}\|^2_{H^{k_\kappa}(\hat{\kappa})}\right]^{1/2}, \tag{20}$$

where C is a positive constant, which is independent of the mesh parameters. Inserting (20) into (19) gives the statement of the Theorem. □

Remark 7.3. *We note that since the fine mesh $\mathcal{T}_{h_\ell}$ is fixed, we have that*

$$h_F \geq \frac{h_\kappa}{2^{\ell-1}}.$$

Thereby, the a priori *error bound derived in Theorem 7.2 may be rewritten in the following form:*

$$|||\,u - u_h\,|||^2_{\mathtt{DG}} \leq C' \sum_{\kappa\in\mathcal{T}_{\mathtt{CFE}}} \frac{h_\kappa^{2(s_\kappa-1)}}{p_\kappa^{2k_\kappa-3}}\|\mathfrak{E}\tilde{u}\|^2_{H^{k_\kappa}(\hat{\kappa})},$$

where $C' = C\,2^{\ell-1}$. *Moreover, for uniform orders* $p_\kappa = p \geq 1$, $s_\kappa = s$, $2 \leq s \leq \min(p+1, k)$, $k \geq 1$, *and* $h = \max_{\kappa \in \mathcal{T}_{\mathtt{CFE}}} h_\kappa$, *we get the bound*

$$|||\, u - u_h \,|||_{\mathtt{DG}} \leq C \frac{h^{s-1}}{p^{k-3/2}} \|\tilde{u}\|^2_{H^k(\Omega)};$$

here, we have employed Theorem 2.1. This bound is optimal in h, *suboptimal in* p *by* $p^{1/2}$, *and coincides with estimates derived in [12] and [15] for so-called standard DG methods.*

8 Implementation

In this section we discuss several aspects concerning the implementation of the DGCFEM. To this end, we first write

$$\mathbf{A}_{\mathtt{CFE}} \mathbf{x}_{\mathtt{CFE}} = \mathbf{f}_{\mathtt{CFE}}$$

to denote the linear system of equations stemming from the discretization of (1)–(2), based on employing the DGCFEM (5), which utilizes the CFE finite element space $V(\mathcal{T}_{\mathtt{CFE}}, \boldsymbol{p})$. Similarly, we write

$$\mathbf{A}_{h_\ell} \mathbf{x}_{h_\ell} = \mathbf{f}_{h_\ell}$$

to denote the linear system of equations which arise from the *standard* DGFEM discretization of problem (1)–(2) based on employing the (standard) finite element space $V(\mathcal{T}_{h_\ell}, p)$ consisting of discontinuous piecewise polynomials of degree p. The entries of the matrix $\mathbf{A}_{\mathtt{CFE}}$ and those of the vector $\mathbf{f}_{\mathtt{CFE}}$ for the CFE method are computed in a different manner to the those for the standard DG method. Indeed, the sparsity of the matrix $\mathbf{A}_{\mathtt{CFE}}$ reflects the topology of the mesh $\mathcal{T}_{\mathtt{CFE}}$; thereby, the actual values of the entries in both the matrix $\mathbf{A}_{\mathtt{CFE}}$ and vector $\mathbf{f}_{\mathtt{CFE}}$ are computed based on aggregating the appropriate entries of $\mathbf{A}_{h_\ell}$ and $\mathbf{f}_{h_\ell}$, respectively. The construction of the CFE space, as described in Section 3, implies that even when the mesh $\mathcal{T}_{\mathtt{CFE}}$ contains just a small number of elements, the supports of the corresponding composite finite element basis functions $\phi_{\mathtt{CFE}}$ which belong to the space $V(\mathcal{T}_{\mathtt{CFE}}, \boldsymbol{p})$ accurately reflect the complexity of the geometry of the underlying computational domain Ω

There are two key aspects related to the construction of the matrix and right-hand side vector $\mathbf{A}_{\mathtt{CFE}}$ and $\mathbf{f}_{\mathtt{CFE}}$, respectively. Firstly, any basis function $\phi_{\mathtt{CFE}}$ which belongs to the space $V(\mathcal{T}_{\mathtt{CFE}}, \boldsymbol{p})$ also belongs to the polynomial space $\mathcal{P}_p(\kappa_{\mathtt{CFE}})$, where $\kappa_{\mathtt{CFE}}$ is the composite finite element domain over which $\phi_{\mathtt{CFE}}$ is defined. Thereby, in case when $p = 1$ and $d = 2$, there are three basis functions $\phi_{\mathtt{CFE},i}$, $i = 1, \ldots, 3$, associated to the element $\kappa_{\mathtt{CFE}}$; here, the index i denotes a local ordering of the basis functions related to $\kappa_{\mathtt{CFE}}$. Secondly, any basis function $\phi_{\mathtt{CFE},i}$, $i = 1, \ldots, \dim(V(\mathcal{T}_{\mathtt{CFE}}, \boldsymbol{p}))$, where i now denotes the global ordering of the basis functions, can be constructed as a linear combination of the basis functions $\phi_{h_\ell,j}$ of $V(\mathcal{T}_{h_\ell}, p)$, i.e.,

$$\phi_{\mathtt{CFE},i} := \sum_{j=1,\ldots,\dim(V(\mathcal{T}_{h_\ell},p))} \alpha_{i,j} \phi_{h_\ell,j} \ , \tag{21}$$

where $\alpha_{i,j}$ are real coefficients which determine how the CFE space $V(\mathcal{T}_{\mathtt{CFE}}, \boldsymbol{p})$ is constructed from the standard finite element space $V(\mathcal{T}_{h_\ell}, p)$. This representation follows immediately, since it is assumed the meshes are nested and that all the children elements of a CFE element $\kappa_{\mathtt{CFE}}$ have the same polynomial degree as $\kappa_{\mathtt{CFE}}$; indeed, we have that $V(\mathcal{T}_{\mathtt{CFE}}, \boldsymbol{p}) \subset V(\mathcal{T}_{h_\ell}, p)$. Writing Λ to denote the set of all coefficients $\alpha_{i,j}$, we deduce from (21) that

$\sharp\Lambda = \dim(V(\mathcal{T}_{h_\ell}, p)) \times \dim(V(\mathcal{T}_{\texttt{CFE}}, \boldsymbol{p}))$. A straightforward consequence of (21) is that any entry $\mathbf{A}_{\texttt{CFE}}[i, r]$ of the matrix $\mathbf{A}_{\texttt{CFE}}$ is simply a linear combination of the entries of $\mathbf{A}_{h_\ell}$; indeed, we note that

$$\begin{aligned} \mathbf{A}_{\texttt{CFE}}[i,j] &= B_{\texttt{DG}}(\phi_{\texttt{CFE},i}, \phi_{\texttt{CFE},j}) := \sum_{m,n=1,\ldots,\dim(V(\mathcal{T}_{h_\ell},p))} \alpha_{i,m}\alpha_{j,n} B_{\texttt{DG}}(\phi_{h_\ell,m}, \phi_{h_\ell,n}) \\ &= \sum_{m,n=1,\ldots,\dim(V(\mathcal{T}_{h_\ell},p))} \alpha_{i,m}\alpha_{j,n}\mathbf{A}_{h_\ell}[m,n] \ . \end{aligned} \tag{22}$$

Similarly, the entries present in the vector $\mathbf{f}_{\texttt{CFE}}$ may be defined in an analogous fashion:

$$\begin{aligned} \mathbf{f}_{\texttt{CFE}}[i] &= F_h(\phi_{\texttt{CFE},i}) := \sum_{j=1,\ldots,\dim(V(\mathcal{T}_{h_\ell},p))} \alpha_{i,j} F_h(\phi_{h_\ell,j}) \\ &= \sum_{j=1,\ldots,\dim(V(\mathcal{T}_{h_\ell},p))} \alpha_{i,j}\mathbf{f}_{h_\ell}[j] \ . \end{aligned} \tag{23}$$

Remark 8.1. *From* (22) *and* (23) *it is clear that in order to construct* $\mathbf{A}_{\texttt{CFE}}$ *and* $\mathbf{f}_{\texttt{CFE}}$*, it is not necessary to store* $\mathbf{A}_{h_\ell}$ *and* $\mathbf{f}_{h_\ell}$*, which would potentially require a large amount of memory; indeed, it is possible to directly construct both* $\mathbf{A}_{\texttt{CFE}}$ *and* $\mathbf{f}_{\texttt{CFE}}$ *from the entries of* $\mathbf{A}_{h_\ell}$ *and* $\mathbf{f}_{h_\ell}$*, respectively, using the above linear combinations determined by the coefficients* $\alpha_{i,j}$*. In this way, the amount of memory required to construct the linear system of equations stemming from the CFE method is essentially just the memory needed to store* $\mathbf{A}_{\texttt{CFE}}$ *and* $\mathbf{f}_{\texttt{CFE}}$ *(which are generally small, compared to* $\mathbf{A}_{h_\ell}$ *and* $\mathbf{f}_{h_\ell}$*) and the coefficients* $\alpha_{i,j}$*. However, the CPU time needed to construct the CFE linear system is clearly dependent on the dimension of the underlying finite element space* $V(\mathcal{T}_{h_\ell}, p)$*.*

As already stated above, the role of the coefficients $\alpha_{i,j}$ is to provide information concerning how the basis functions $\phi_{\texttt{CFE},i}$ present in the coarse space $V(\mathcal{T}_{\texttt{CFE}}, \boldsymbol{p})$ are defined in terms of the basis functions defined on the finer space $V(\mathcal{T}_{h_\ell}, p)$. We remark that this construction is element-wise in the sense that for each element $\kappa \in V(\mathcal{T}_{h_\ell}, p)$, there is a subset of coefficients $\Lambda_\kappa \subset \Lambda$, such that the corresponding linear combination of the basis functions defined on κ, reconstruct the restriction of the basis functions defined on the father element $\kappa_{\texttt{CFE}}$ to κ. Repeating this process for all children κ of $\kappa_{\texttt{CFE}}$, we are able to entirely reconstruct the basis functions of the coarse space defined on $\kappa_{\texttt{CFE}}$. Since it is assumed that the same order of polynomials p are used on both κ and its father, we have that $\sharp\Lambda_\kappa = n_\kappa^2$, where n_κ denotes the dimension of the local polynomial space on element κ; i.e., $n_\kappa = p_\kappa(p_\kappa + 1)/2$ in the case when triangular elements are used in two–dimensions, for example. An interesting property of these coefficients $\alpha_{i,j}$ is that they are completely independent of the underlying PDE problem at hand, but only depend on the two finite element spaces $V(\mathcal{T}_{\texttt{CFE}}, \boldsymbol{p})$ and $V(\mathcal{T}_{h_\ell}, p)$. We write $\phi_{\texttt{CFE},\kappa_{\texttt{CFE}},i}$, $i = 1, \ldots, \dim(\mathcal{P}_p(\kappa_{\texttt{CFE}}))$, to denote the basis functions defined over element $\kappa_{\texttt{CFE}} \in \mathcal{T}_{\texttt{CFE}}$; similarly, $\phi_{h_\ell,\kappa,j}$, $j = 1, \ldots, \dim(\mathcal{P}_p(\kappa))$, denotes the corresponding set of basis functions associated with element $\kappa \in \mathcal{T}_{h_\ell}$. Given that $\kappa_{\texttt{CFE}} \in \mathcal{T}_{\texttt{CFE}}$ is defined as the union of their child elements present in $\mathcal{T}_{h_\ell}$, the intersection between the support of a basis function $\phi_{\texttt{CFE},\kappa_{\texttt{CFE}},i}$ defined over $\kappa_{\texttt{CFE}}$ and a basis function $\phi_{h_\ell,\kappa,j}$ defined on $\kappa \in \mathcal{T}_{h_\ell}$ is zero unless the element κ is a child of $\kappa_{\texttt{CFE}}$; if this latter condition is not satisfied, then clearly, the corresponding coefficients present in $\alpha_{i,j}$ be identically equal to zero. This observation dramatically reduces the number of coefficients that need to be computed; indeed, we may

characterize the coefficients that may be non-zero as follows

$$\Lambda_0 := \bigcup_{\kappa \in \mathcal{T}_{h_l}} \Lambda_\kappa \ , \quad \Lambda_0 \subset \Lambda \ ,$$

which implies that $\sharp\Lambda_0 = \sum_{\kappa \in \mathcal{T}_{h_l}} n_\kappa^2 < \sharp\Lambda$.

The most general way to compute the coefficients Λ_0 is by solving a family of square linear systems $\mathcal{R}$. The family $\mathcal{R}$ can be split in subfamilies $\mathcal{R}_\kappa$, one for each element $\kappa \in \mathcal{T}_{h_\ell}$. All the linear systems in the same subfamily $\mathcal{R}_\kappa$ are characterized to have the same matrix, but a different right-hand side. This can be exploited, for example, when an LU decomposition is used to solve all the linear systems in the family, since even if there are as many linear systems to solve as the number of elements in $\mathcal{T}_{h_\ell}$ times the dimension of the space $V(\mathcal{T}_{\texttt{CFE}}, \boldsymbol{p})$, only as many LU decompositions as the number of elements in $\mathcal{T}_{h_\ell}$ are needed. Denoting by $\kappa_{\texttt{CFE}}$ the father of an element κ, and by $\{\alpha_{i,j}\}$ the set of coefficients corresponding to the basis functions of the two elements, we have that the linear systems in the subfamily of κ have the form

$$\mathbf{C}_\kappa \boldsymbol{\alpha}_{\kappa,i} = \boldsymbol{\phi}_{\kappa,i} \ ,$$

where $\boldsymbol{\alpha}_{\kappa,i}$ is the vector containing the unknown coefficients Λ_κ to reconstruct the basis function $\phi_{\texttt{CFE},\kappa_{\texttt{CFE}},i}$ on the support of κ, the matrix $\mathbf{C}_\kappa$ is the same for any $\phi_{\texttt{CFE},\kappa_{\texttt{CFE}},i}$ and $\boldsymbol{\phi}_{\kappa,i}$ depends on the restriction of $\phi_{\texttt{CFE},\kappa_{\texttt{CFE}},i}$ to κ. The dimension of the linear systems in the subfamily is equal to the number of basis functions of the element κ, which is the same as the number of basis functions of its father element $\kappa_{\texttt{CFE}}$, due to the constraint on the choice of polynomial orders we imposed between the two meshes.

In order to define the matrices $\mathbf{C}_\kappa$ and vectors $\boldsymbol{\phi}_{\kappa,i}$, we need do define a set of points $\mathcal{Q}_{\kappa,p}$, for each element κ, whose cardinality depends on the order of the approximating polynomial p on the element. As an example, let κ_{ref} be the reference triangle with vertices $(0,0)$, $(1,0)$ and $(0,1)$; moreover let $\mathcal{Q}_s$, with $s \in \mathbb{R}_+$, be the set of all points $\mathbf{q}$ in the real plane such that $q := (ns\mathbf{e}_1, ms\mathbf{e}_2)$, with $n, m \in \mathbb{N}$ and $\mathbf{e}_1, \mathbf{e}_2$ is the canonical basis of $\mathbb{R}^2$. Then the set $\mathcal{Q}_{\kappa,p}$ is defined as:

$$\mathcal{Q}_{\kappa,p} := \mathcal{A}_\kappa(\mathcal{Q}_{1/p} \cap \kappa_{\text{ref}}) \ ,$$

where $\mathcal{A}_\kappa$ is the affine transformation which maps κ_{ref} into κ. The points present in $\mathcal{Q}_{\kappa,p}$, define where the basis functions $\phi_{\texttt{CFE},\kappa_{\texttt{CFE}},i}$, $\phi_{h_\ell,\kappa,j}$ are evaluated in order to assemble the matrices $\mathbf{C}_\kappa$ and the vectors $\boldsymbol{\phi}_\kappa$. Indeed, for any κ and any $\phi_{\texttt{CFE},\kappa_{\texttt{CFE}},i}$ the vector $\boldsymbol{\phi}_\kappa$ is given by

$$\boldsymbol{\phi}_{\kappa,i}[j] := \phi_{\texttt{CFE},\kappa_{\texttt{CFE}},i}(q_j) \quad \forall q_j \in \mathcal{Q}_{\kappa,p} \ .$$

Similarly, for any κ, the matrix $\mathbf{C}_\kappa$ is defined as

$$\mathbf{C}_\kappa[r,j]; = \phi_{h_\ell,\kappa,r}(q_j) \quad \forall q_j \in \mathcal{Q}_{\kappa,p} \ \forall \phi_{h_\ell,\kappa,r} \ .$$

The computation of the solutions of all these linear systems can be quite expensive; however, this process may be undertaken in a more efficient manner. To this end, suppose for the moment that both finite element spaces $V(\mathcal{T}_{\texttt{CFE}}, \boldsymbol{p})$ and $V(\mathcal{T}_{h_\ell}, p)$ employ a set of nodal Lagrange basis function on each element. Then, it follows straightforwardly, from the properties of the nodal basis functions and the definitions of the sets $\mathcal{Q}_{\kappa,p}$, that all matrices $\mathbf{C}_\kappa$ reduce to the identity matrix. Thereby, in this case, we conclude that

$$\boldsymbol{\alpha}_{\kappa,i} \equiv \boldsymbol{\phi}_{\kappa,i} \ ;$$

in this case the computation of the coefficients in Λ_0, simply requires the evaluation of the basis functions $\phi_{\mathtt{CFE},i}$ at the nodes determined by the sets $\mathcal{Q}_{\kappa,p}$. With this observation, more general modal bases may be considered, with only a small computational overhead. Indeed, suppose that for any p, $\mathbf{B}_p$ is the matrix that transforms the nodal polynomial basis for $\mathcal{P}_p$ into an alternative basis which spans the same polynomial space, such as a modal basis, for example. Since these matrices $\mathbf{B}_p$ are invariant under affine transformations, they can be computed just for the reference element in advance and stored. Now, if for the example when modal basis functions are employed within both finite element spaces $V(\mathcal{T}_{\mathtt{CFE}}, \boldsymbol{p})$ and $V(\mathcal{T}_{h_\ell}, p)$, then the components of the systems $\tilde{\mathbf{C}}_\kappa \tilde{\boldsymbol{\alpha}}_{\kappa,i} = \tilde{\boldsymbol{\phi}}_{\kappa,i}$ for the modal basis functions are equivalent to the components of the systems for the nodal basis functions in the following manner:

$$\mathbf{C}_\kappa \equiv \mathbf{B}_p^{-1} \tilde{\mathbf{C}}_\kappa \mathbf{B}_p \ , \quad \boldsymbol{\phi}_{\kappa,i} \equiv \mathbf{B}_p^{-1} \tilde{\boldsymbol{\phi}}_{\kappa,i} \ ,$$

i.e., $\tilde{\boldsymbol{\alpha}}_{\kappa,i} := \mathbf{B}_p \boldsymbol{\alpha}_{\kappa,i}$. This approach is extremely cheap, since it does not require the inversion of a linear system of equations; indeed, the matrices $\mathbf{B}_p$ can be all precomputed and stored, since they are independent of the underlying PDE problem.

9 Numerical experiments

In this section we present a series of computational examples to numerically investigate the asymptotic convergence behaviour of the proposed DGCFEM for problems where the underlying computational domain contains micro-structures. Throughout this section the DGCFEM solution u_h defined by (5) is computed with the constant γ appearing in the interior penalty parameter σ defined by (6) equal to 10. All the numerical examples presented in this section have been computed using the AptoFEM package (`www.aptofem.com`); here, the resulting system of linear equations is solved based on employing the Multifrontal Massively Parallel Solver (MUMPS), see [1, 2, 3].

9.1 Two–dimensional domain with a complicated boundary

In this first example, we consider a computational domain with a complicated boundary; to this end, we let Ω be the unit square in two–dimensions, where a series of tiny 'finger–like' cuts have been removed from the right-hand boundary, i.e., where $x = 1$, $0 \leq y \leq 1$. More precisely, the right-hand side boundary of the domain possesses 64 equidistributed tiny 'gaps'; cf. Figure 2. In this example, we select the right-hand side forcing function f and appropriate inhomogeneous boundary condition $u = g$ on $\partial\Omega$, so that the analytical solution to (1)–(2) is given by $u = \tanh(2x)$.

In order to compute the numerical approximation to (1)–(2) using the DGCFEM defined in (5), we first construct a sequence of meshes based on employing Algorithm 3.1. To this end, the coarsest mesh reference mesh $\hat{\mathcal{T}}_H$ is selected to be a uniform triangular mesh; in particular, the coarsest mesh is constructed from a uniform 2×2 square mesh by connecting the north east vertex with the south west one within each mesh square, cf. Figure 2(a). This mesh is then subsequently adaptively refined in order to generate a fine reference mesh consisting of 20160 triangular elements, which precisely describes the computational domain Ω. Here, we point out that the choice of the initial triangulation and the definition of Ω have been selected so that Ω may be exactly triangulated using Algorithm 3.1, without the need

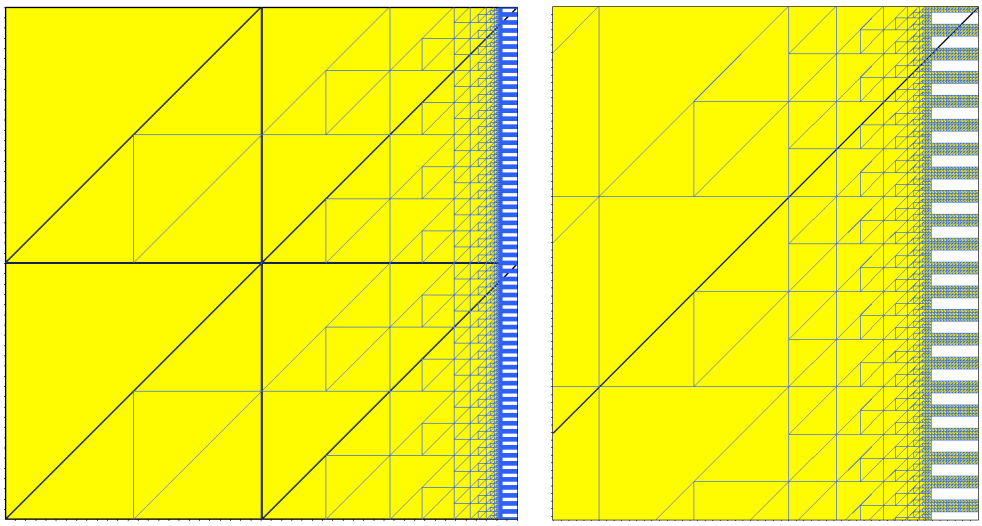

(a) (b)

Figure 2: Example 1: (a) Initial composite finite element mesh. The colour blue denotes elements present in the fine level mesh (which consists of 20160 triangular elements); elements plotted in black form the coarse level mesh (containing 8 elements); finally, the domain Ω is shown in yellow. (b) Zoom of (a).

to move any nodal points in the finest reference mesh. Thereby, in this setting, the respective hierarchy of logical and physical meshes are both identical.

Eles	Dofs	$\|u-u_h\|_{L_2(\Omega)}$	k	$\|u-u_h\|_{1,h}$	k	$\|\|\|u-u_h\|\|\|_{\mathtt{DG}}$	k
8	24	2.498E-02	-	3.122E-01	-	4.334E-01	-
32	96	6.336E-03	1.98	1.461E-01	1.10	1.693E-01	1.36
128	384	1.615E-03	1.97	7.207E-02	1.02	7.825E-02	1.11
512	1536	3.914E-04	2.04	3.582E-02	1.01	3.801E-02	1.04
2048	6144	1.038E-04	1.91	1.788E-02	1.00	1.885E-02	1.01
8192	24576	2.592E-05	2.00	8.944E-03	1.00	9.313E-03	1.02

Table 1: Example 1: Convergence of the DGCFEM on a sequence of uniform triangular composite elements with $p = 1$.

We now investigate the asymptotic convergence of the proposed DGCFEM on a sequence of successively finer uniform triangular meshes, starting with $\mathcal{T}_{\mathtt{CFE}}$ consisting of 8 composite elemental domains, for $p = 1, 2$; see Tables 1 & 2, respectively. In each case we show the number of elements (Eles) and number of degrees of freedom (Dofs) in the composite finite element space $V(\mathcal{T}_{\mathtt{CFE}}, \boldsymbol{p})$, the $L_2(\Omega)$, the broken $H^1(\Omega)$-semi-norm (denoted by $|\cdot|_{1,h}$) and the DG–norm of the error $u-u_h$, together with their respective rates of convergence, denoted by k in each case. We remark that none of the (composite) finite element meshes employed here are fine enough to exactly represent the computational domain Ω.

From Tables 1 & 2, we observe that both the $L_2(\Omega)$ norm and broken $H^1(\Omega)$ seminorm of the error converge at the expected optimal rate, even in the presence of such micro-structure

Eles	Dofs	$\|u-u_h\|_{L_2(\Omega)}$	k	$\|u-u_h\|_{1,h}$	k	$\|\|\|u-u_h\|\|\|_{\mathtt{DG}}$	k
8	48	4.744E-03	-	4.998E-02	-	7.600E-02	-
32	192	5.870E-04	3.01	1.553E-02	1.69	2.038E-02	1.90
128	768	7.512E-05	2.97	3.924E-03	1.98	4.754E-03	2.10
512	3072	1.228E-05	2.61	9.881E-04	1.99	1.119E-03	2.09
2048	12288	1.108E-06	3.47	2.446E-04	2.01	2.717E-04	2.04
8192	49152	1.398E-07	2.99	6.124E-05	2.00	6.598E-05	2.04

Table 2: Example 1: Convergence of the DGCFEM on a sequence of uniform triangular composite elements with $p = 2$.

present in the boundary of the computational domain Ω. More precisely, we observe that $\|u-u_h\|_{L_2(\Omega)}$ and $|u-u_h|_{1,h}$ converge to zero like $\mathcal{O}(h^{p+1})$ and $\mathcal{O}(h^p)$, respectively, for each fixed p, as h tends to zero. In terms of the convergence of the DGCFEM with respect to the DG–norm, we observe the convergence rate $\mathcal{O}(h^p)$, as h tends to zero, for each fixed p; this corresponds to the expected rate of convergence of the so-called *standard* DGFEM, cf. [4], for example, in the absence of micro-structures. The observed rate of convergence of the DGCFEM with respect to the DG–norm is in accordance with Theorem 7.2, since most elements κ in the composite finite element mesh $\mathcal{T}_{\mathtt{CFE}}$ are 'standard' element domains (triangles in this case), except for a relatively small number which lie in the vicinity of the right-hand side boundary of the domain Ω; thereby, for such elements, we have $h_F = h_\kappa$.

9.2 Two–dimensional domain with micro-structures

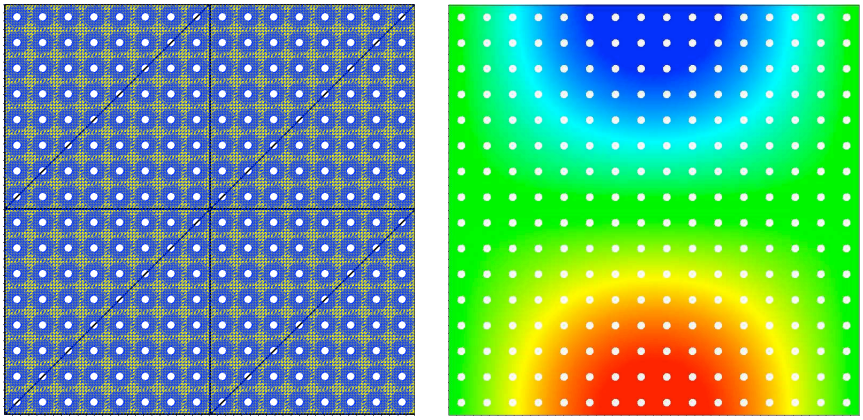

(a) (b)

Figure 3: Example 2: (a) Initial composite finite element mesh. The colour blue denotes elements present in the fine level mesh (which consists of 85500 triangular elements); elements plotted in black form the coarse level mesh (containing 8 elements); finally, the domain Ω is shown in yellow. (b) Analytical solution.

In this second example, we consider the case when the computational domain Ω contains a large number of small geometric features. To this end, we set Ω to be the unit square $(0,1)^2$ in two-dimensions, which has had a series of uniformly spaced circular holes removed; here, we

consider the case where 256 small circular holes are removed from $(0,1)^2$, see Figure 3(a). In this example, we select the right-hand side forcing function f and appropriate inhomogeneous boundary condition $u = g$ on $\partial\Omega$, so that the analytical solution to (1)–(2) is given by $u = \sin(\pi x)\cos(\pi y)$, cf. Figure 3(b).

As in the previous example, we first define the coarsest reference mesh $\hat{\mathcal{T}}_H$ to be a uniform triangular mesh consisting of 8 elements. This mesh is then refined to generate a sequence of reference meshes according to Algorithm 3.1. Given that the underlying geometry cannot be exactly represented by such a sequence of refined meshes, nodes close to the boundary are moved in order to provide an accurate description of the computational domain. Thereby, in this setting the corresponding sequence of physical meshes differ from their respective logical and reference meshes. Here, the fine mesh consists of 85500 triangular elements; in particular, edges of elements present in the fine mesh which have nodes on one of the circular holes are curved using a local quadratic representation of the edge. We remark that, to avoid 'cracks' appearing in the finest mesh in the vicinity of the holes present in Ω when nodes are locally moved, additional refinement has been undertaken near the circular boundaries.

Eles	Dofs	$\|u-u_h\|_{L_2(\Omega)}$	k	$\|u-u_h\|_{1,h}$	k	$\|\|\|u-u_h\|\|\|_{\mathtt{DG}}$	k
8	24	7.320E-02	-	1.186	-	31.500	-
32	96	2.120E-02	1.78	7.051E-01	0.75	8.314	1.92
128	384	6.214E-03	1.77	3.903E-01	0.85	1.639	2.34
512	1536	2.834E-03	1.13	2.144E-01	0.86	3.342E-01	2.29
2048	6144	4.427E-04	2.68	1.020E-01	1.07	1.201E-01	1.48

Table 3: Example 2: Convergence of the DGCFEM on a sequence of uniform triangular composite elements with $p = 1$.

Eles	Dofs	$\|u-u_h\|_{L_2(\Omega)}$	k	$\|u-u_h\|_{1,h}$	k	$\|\|\|u-u_h\|\|\|_{\mathtt{DG}}$	k
8	48	1.699E-02	-	4.089E-01	-	13.447	-
32	192	2.477E-03	2.78	1.078E-01	1.92	1.941	2.79
128	768	5.734E-04	2.11	3.739E-02	1.53	3.159E-01	2.62
512	3072	1.531E-04	1.91	1.288E-02	1.54	3.208E-02	3.30
2048	12288	1.088E-05	3.81	2.212E-03	2.54	2.515E-03	3.67

Table 4: Example 2: Convergence of the DGCFEM on a sequence of uniform triangular composite elements with $p = 2$.

In Tables 3 & 4 we investigate the asymptotic convergence of the proposed DGCFEM on a sequence of successively finer uniform triangular meshes, starting with $\mathcal{T}_{\mathtt{CFE}}$ consisting of 8 composite elemental domains, for $p = 1, 2$, respectively. As in the previous example, we compute the $L_2(\Omega)$, the broken $H^1(\Omega)$-semi-norm and the DG–norm of the error $u - u_h$, together with their respective rates of convergence. For this example, the rates of convergence are less consistent than those reported in the previous example. For both $p = 1$ and $p = 2$, the quantities $\|u-u_h\|_{L_2(\Omega)}$ and $|u-u_h|_{1,h}$ appear to convergence slightly sub-optimally, excluding on the last mesh, relative to what we would expect. In order to assess the quality of the computed DGCFEM solution, in Figure 4 we compare the proposed DGCFEM with the standard

DGFEM; in the latter case, we simply compute the numerical solution on the unit square $(0,1)^2$ *without* any holes. Here, we now observe that the accuracy and rate of convergence of the DGCFEM, which takes into account the holes present in the computational domain, is very similar to the standard DGFEM which cannot treat the micro-structures present in Ω on such coarse meshes. Indeed, this clearly illustrates that the presence holes/micro-structures in the computational domain does *not* lead to a degradation in the quality of the computed solution when the DGCFEM is exploited. Finally, Tables 3 & 4 indicate that the DG-norm of the error in the DGCFEM solution converges to zero at a faster rate than we would expect for the standard DGFEM. This is in accordance with Theorem 7.2, due to the definition of h_F; indeed, as noted in Remark 4.1, h_F may be selected to be equal to the element dimension only on 'standard' element domains, while on composite element domains, we must select h_F to be equal to the size of the elements present in the fine mesh. For this latter choice, h_F is effectively fixed as the composite finite element mesh is refined; thereby, the order of convergence of the DGCFEM with respect to the DG-norm may exceed the standard predicted order of $\mathcal{O}(h^p)$, cf. Theorem 7.2.

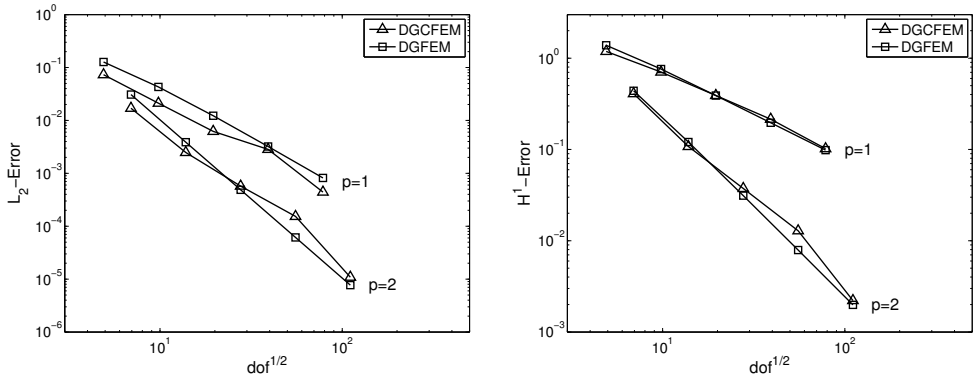

Figure 4: Example 2. Comparison between the DGCFEM and the standard DGFEM (computed without any holes): (a) $\|u - u_h\|_{L_2(\Omega)}$; (b) $|u - u_h|_{1,h}$.

9.3 Three–dimensional domain with micro-structures

In this final example, we consider a three–dimensional problem which contains a number of holes. More precisely, we let Ω to be the unit cube $(0,1)^3$ which has had 16 rectangular sections removed; cf. Figure 5. We point out that the holes only go to a depth of a half of the domain width. We select the right-hand side forcing function f and appropriate inhomogeneous boundary condition $u = g$ on $\partial\Omega$, so that the analytical solution to (1)–(2) is given by $u = \sin(\pi x)\cos(\pi y)\sin(\pi z)$.

Here, the coarsest mesh reference mesh $\hat{\mathcal{T}}_H$ is selected to be a uniform tetrahedral mesh; in particular, the coarsest mesh is constructed from a uniform $2 \times 2 \times 2$ hexahedral mesh by subdividing each hexahedral element into 6 tetrahedra. This mesh is then subsequently adaptively refined in order to generate a fine reference tetrahedral mesh consisting of 21504 elements, which precisely describes the computational domain Ω. Here, we point out that the choice of the initial mesh and the definition of Ω have been selected so that Ω may be exactly triangulated using Algorithm 3.1, without the need to move any nodal points in the

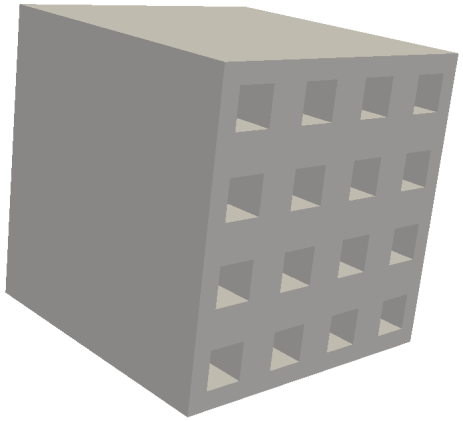

Figure 5: Computational domain Ω.

Eles	Dofs	$\|u-u_h\|_{L_2(\Omega)}$	k	$\|u-u_h\|_{1,h}$	k	$\|\|\| u-u_h \|\|\|_{\mathtt{DG}}$	k
48	192	8.826E-02	-	1.315	-	5.875	-
384	1536	2.905E-02	1.60	8.624E-01	0.61	1.927	1.61
3072	12288	8.664E-03	1.75	4.270E-01	1.01	6.194E-01	1.64
21504	86016	2.582E-03	1.75	2.168E-01	0.98	2.540E-01	1.29

Table 5: Example 3: Convergence of the DGCFEM on a sequence of uniform triangular composite elements with $p = 1$.

Eles	Dofs	$\|u-u_h\|_{L_2(\Omega)}$	k	$\|u-u_h\|_{1,h}$	k	$\|\|\| u-u_h \|\|\|_{\mathtt{DG}}$	k
48	480	2.707E-02	-	5.577E-01	-	2.931	-
384	3840	5.075E-03	2.42	1.770E-01	1.66	4.557E-01	2.69
3072	30720	5.983E-04	3.08	4.288E-02	2.05	6.015E-02	2.92
21504	215040	7.401E-05	3.01	1.076E-02	1.99	1.250E-02	2.27

Table 6: Example 3: Convergence of the DGCFEM on a sequence of uniform triangular composite elements with $p = 2$.

finest reference mesh. The asymptotic convergence of the proposed DGCFEM on a sequence of successively finer uniform tetrahedral meshes, starting with $\mathcal{T}_{\mathtt{CFE}}$ consisting of 48 composite elemental domains, for $p = 1, 2$ is investigated Tables 5 & 6, respectively. Here, we observe that the $L_2(\Omega)$–norm of the error converges at a slightly sub-optimal rate for $p = 1$, though $|u - u_h|_{1,h}$ tends to zero at roughly the optimal rate of $\mathcal{O}(h^p)$, for each fixed p, as the mesh is uniformly refined. As in the previous example, the DG–norm of the error again converges to zero, as the mesh is refined, at a slightly faster rate compared to the expected rate when the standard DGFEM is employed, cf. Theorem 7.2.

10 Concluding remarks

In this article we have considered the extension of the composite finite element technique, originally developed for the standard Galerkin finite element method, to the case when discontinuous finite element spaces are employed. This new class of methods are very attractive as they allow for the numerical approximation of PDE problems posed on complicated domains which contain local geometrical features in an efficient manner. In this article we have undertaken the *a priori* error analysis of the proposed DGCFEM, based on generating a hierarchy of meshes, such that the finest mesh does indeed provide an accurate representation of the underlying computational domain. The finite element spaces can then be defined in a very natural manner, based on employing appropriate prolongation operators. The approach here is to recover finite element spaces, such that on each composite element the numerical solution is a polynomial; by selecting alternative prolongation operators, cf. [11], for example, finite element basis functions which are piecewise polynomial on each composite element may also be defined. Numerical experiments highlighting the application of the proposed DGCFEM for a range of two– and three–dimensional problems have been presented. Future work will be concerned with the *a posteriori* error analysis of DGCFEMs, as well as the application of DGCFEMs within two–level Schwarz–type preconditioners.

Acknowledgements

SG and PH acknowledge the financial support of the EPSRC under the grant EP/H005498.

References

[1] P. R. Amestoy, I. S. Duff, J. Koster, and J.-Y. L'Excellent. A fully asynchronous multifrontal solver using distributed dynamic scheduling. *SIAM Journal on Matrix Analysis and Applications*, 23(1):15–41, 2001.

[2] P. R. Amestoy, I. S. Duff, and J.-Y. L'Excellent. Multifrontal parallel distributed symmetricand unsymmetric solvers. *Comput. Methods Appl. Mech. Eng.*, 184:501–520, 2000.

[3] P. R. Amestoy, A. Guermouche, J.-Y. L'Excellent, and S. Pralet. Hybrid scheduling for the parallel solution of linear systems. *Parallel Computing*, 32(2):136–156, 2006.

[4] D.N. Arnold, F. Brezzi, B. Cockburn, and L.D. Marini. Unified analysis of discontinuous Galerkin methods for elliptic problems. *SIAM J. Numer. Anal.*, 39:1749–1779, 2001.

[5] I. Babuška and M. Suri. The *hp*–version of the finite element method with quasiuniform meshes. *RAIRO Anal. Numér.*, 21:199–238, 1987.

[6] E. Burman and P. Hansbo. Fictitious domain finite element methods using cut elements: I. A stabilized Lagrange multiplier method. *Comput. Methods Appl. Mech. Engrg.*, 199:2680–2686, 2010.

[7] E. Burman and P. Hansbo. An interior-penalty-stabilized Lagrange multiplier method for the finite-element solution of elliptic interface problems. *IMA J. Numer. Anal.*, 30:870–885, 2010.

[8] E. Burman and P. Hansbo. Fictitious domain finite element methods using cut elements: II. A stabilized Nitsche method. *Appl. Numer. Math.*, 62:328–341, 2012.

[9] E.H. Georgoulis, E. Hall, and P. Houston. Discontinuous Galerkin methods for advection–diffusion–reaction problems on anisotropically refined meshes. *SIAM J. Sci. Comput.*, 30(1):246–271, 2007.

[10] W. Hackbusch and S.A. Sauter. Composite finite elements for problems containing small geometric details. Part II: Implementation and numerical results. *Comput. Visual Sci.*, 1:15–25, 1997.

[11] W. Hackbusch and S.A. Sauter. Composite finite elements for the approximation of PDEs on domains with complicated micro-structures. *Numer. Math.*, 75:447–472, 1997.

[12] P. Houston, C. Schwab, and E. Süli. Discontinuous *hp*-finite element methods for advection–diffusion–reactio n problems. *SIAM J. Numer. Anal.*, 39:2133–2163, 2002.

[13] A. Johansson and M.G. Larson. A high order discontinuous Galerkin Nitsche method for elliptic problems with fictitious boundary. *Submitted for publication*, 2011.

[14] M. Rech, S. Sauter, and A. Smolianski. Two-scale composite finite element method for the Dirichlet problem on complicated domains. *Numer. Math.*, 102(4):681–708, 2006.

[15] B. Rivière, M.F. Wheeler, and V. Girault. Improved energy estimates for interior penalty, constrained and discontinuous Galerkin methods for elliptic problems, Part I. *Comput. Geosci.*, 3:337–360, 1999.

[16] S. A. Sauter and R. Warnke. Extension operators and approximation on domains containing small geometric details. *East-West J. Numer. Math.*, 7(1):61–77, 1999.

[17] G.H. Shortley and R. Weller. Numerical solution of laplaces equation. *J. Appl. Phys*, 9:334–348, 1938.

[18] E. M. Stein. *Singular Integrals and Differentiability Properties of Functions*. Princeton, University Press, Princeton, N.J., 1970.

[19] E. Süli, Ch. Schwab, and P. Houston. *hp*–DGFEM for partial differential equations with nonnegative characteristic form. In B. Cockburn, G.E. Karniadakis, and C.-W. Shu, editors, *Discontinuous Galerkin Methods: Theory, Computation and Applications, Lecture Notes in Computational Science and Engineering, Vol. 11*, pages 221–230. Springer, 2000.

MOX Technical Reports, last issues

Dipartimento di Matematica "F. Brioschi",
Politecnico di Milano, Via Bonardi 9 - 20133 Milano (Italy)

23/2012 Fabio Nobile, Christian Vergara
Partitioned algorithms for fluid-structure interaction problems in haemodynamics

24/2012 Antonietti, P.F.; Giani, S.; Houston, P.
hpVersion Composite Discontinuous Galerkin Methods for Elliptic Problems on Complicated Domains

22/2012 Ettinger, B.; Passerini, T.;Perotto, S.; Sangalli, L.M.
Regression models for data distributed over non-planar domains

21/2012 Guglielmi, A.; Ieva, F.; Paganoni, A.M.; Ruggeri, F.; Soriano, J.
Semiparametric Bayesian models for clustering and classification in presence of unbalanced in-hospital survival

20/2012 Ieva, F.; Paganoni, A. M.; Zanini, P.
Statistical models for detecting Atrial Fibrillation events

19/2012 Faggiano, E.; Antiga, L.; Puppini, G.; Quarteroni, A.; Luciani G.B.; Vergara, C.
Helical Flows and Asymmetry of Blood Jet in Dilated Ascending Aorta with Normally Functioning Bicuspid Valve

18/2012 Formaggia, L.; Vergara, C.
Prescription of general defective boundary conditions in fluid-dynamics

17/2012 Manzoni, A.; Quarteroni, A.; Gianluigi Rozza, G.
Computational reduction for parametrized PDEs: strategies and applications

16/2012 Cutri', E.; Zunino, P.; Morlacchi, S.; Chiastra, C.; Migliavacca, F.
Drug delivery patterns for different stenting techniques in coronary bifurcations: a comparative computational study

15/2012 Mengaldo, G.; Tricerri, P.; Crosetto,P.; Deparis, S.; Nobile, F.; Formaggia, L.
A comparative study of different nonlinear hyperelastic isotropic arterial wall models in patient-specific vascular flow simulations in the aortic arch